A Versatile and Reproducible Cryo-sample Preparation Methodology for Atom Probe Studies

Eric V Woods, Mahander P Singh, Se-Ho Kim, Tim M Schwarz, James O Douglas, Ayman A El-Zoka, Finn Giulani, Baptiste Gault

Microscopy and Microanalysis, 2023, **00**, 1–12
https://doi.org/10.1093/micmic/ozad120

Original Article

Microscopy AND Microanalysis

A Versatile and Reproducible Cryo-sample Preparation Methodology for Atom Probe Studies

Eric V. Woods[1,a], Mahander P. Singh[1,a], Se-Ho Kim[1], Tim M. Schwarz[1], James O. Douglas[2], Ayman A. El-Zoka[1,2], Finn Giulani[2], and Baptiste Gault[1,2,*]

[1]*Mikrostrukturphysik und Legierungsdesign, Max-Planck-Institut für Eisenforschung GmbH, Max-Planck-Straße 1, Düsseldorf 40237, Germany*
[2]*Department of Materials, Royal School of Mines, Imperial College London, Prince Consort Road, London SW7 2BP, UK*

***Corresponding author:** Baptiste Gault, Email: b.gault@mpie.de

[a]Eric V. Woods and Mahander P. Singh equally contributed to the present study and can be regarded, therefore, as being main authors.

Abstract

Repeatable and reliable site-specific preparation of specimens for atom probe tomography (APT) at cryogenic temperatures has proven challenging. A generalized workflow is required for cryogenic specimen preparation including lift-out via focused ion beam and *in situ* deposition of capping layers, to strengthen specimens that will be exposed to high electric field and stresses during field evaporation in APT and protect them from environment during transfer into the atom probe. Here, we build on existing protocols and showcase preparation and analysis of a variety of metals, oxides, and supported frozen liquids and battery materials. We demonstrate reliable *in situ* deposition of a metallic capping layer that significantly improves the atom probe data quality for challenging material systems, particularly battery cathode materials which are subjected to delithiation during the atom probe analysis itself. Our workflow design is versatile and transferable widely to other instruments.

Key words: atom probe tomography, battery cathodes, cryo-focused ion beam, frozen liquids

Introduction

Atom probe tomography (APT) offers a unique combination of high spatial resolution and elemental sensitivity in the atomic part-per-million range, to provide three-dimensional analysis of the distribution of atoms in a material (Gault et al., 2021; Lim et al., 2020; De Geuser & Gault, 2020; Devaraj et al., 2018). The overall process involves generating high electric fields at the end of a needle-shaped specimen, typically <100 nm in diameter, that cause the joint ionization and desorption of atoms from the surface, triggered by either laser or voltage pulses (Gault et al., 2006; Hono et al., 2011). These needle-shaped specimens are routinely prepared using dual-beam scanning electron microscopes-focused ion beams (SEM-FIB) (Thompson et al., 2007; Prosa & Larson, 2017). However, the FIB-based preparation of beam-sensitive materials or liquid samples remains challenging (Schreiber et al., 2018; Bassim et al., 2012). Cryogenic freezing can preserve the sample's structure and composition, enabling high-quality analysis while minimizing FIB milling-induced damage (McCarroll et al., 2020; El-Zoka et al., 2020; Rivas et al., 2020). The development of cryogenic stages for the SEM-FIBs has enabled the analysis of a wider range of materials using APT, and cryogenic shuttle systems allow for the transfer of specimens between instruments, enabling APT analysis of materials that are sensitive to air or change in temperatures (Gerstl & Wepf, 2015; Perea et al., 2017; Stephenson et al., 2018).

These developments have facilitated APT studies of hydrogen in steel (Chen et al., 2017) and aluminum (Zhao et al., 2022), elemental distributions in battery materials (Singh et al., 2023; Li et al., 2022), and frozen liquids and their interface with a metallic substrate (Schreiber et al., 2018; Schwarz et al., 2020; El-Zoka et al., 2020; *Kim, Stephenson, et al., 2022*). Cryogenic techniques for preparing frozen liquid specimen for APT analysis are still under development, but they offer a promising approach for characterizing the distribution of species in solutions. However, further research and development is required to fully realize the potential of this approach.

One of the inherent difficulties in preparing specimens at cryogenic temperatures is the uncontrolled deposition introduced by the gas injection system (GIS) without decomposing the precursor species. This uncontrolled deposition makes the process of site-specific lift-out and mounting the specimen onto the support a highly challenging process, often resulting in high rate of failures (Prosa & Larson, 2017). Furthermore, the organic and metalo-organic precursor vapors produced by the GIS tend to condensate over the entire cooled surface, leading to the formation of a potentially thick coating (Parmenter, et al., 2014). This coating complicates the preparation of specimens further, making it more challenging to locate a region of interest (ROI), requiring extra efforts to mill-out and shape the final APT specimens (Perea, et al., 2019).

In recent years, alternative approaches for preparing samples at cryogenic temperatures have been investigated. FIB-free methods have been developed, such as embedding the liquids between a metallic specimen and graphene layers (Qiu et al., 2020; Zhang et al., 2022), making specimens from frozen liquids on a flat substrate (El-Zoka et al., 2020) or on a wire (Schwarz et al., 2020; Stender et al., 2022), or

Received: March 31, 2023. **Revised:** August 14, 2023. **Accepted:** October 1, 2023

infiltrating the liquid into a porous structure (Kim, El-Zoka, et al., 2022). The liquid used as a carrier for biological material should ideally be vitrified, in order to avoid damage related to the volume change caused by crystallization. For water to be frozen in an amorphous, glassy ice phase, it requires cooling rates of $\sim 10^5$ K/min (Cavalier, et al., 2008; Dubochet & McDowall, 1981; Marko, et al., 2006). The abovementioned approaches have shown promise, but they face severe limitations with respect to the volume that can be encapsulated, the lack of control of the freezing rate to ensure vitrification in liquid samples, and the impossibility to select an ROI.

FIB preparations of beam-sensitive samples, including battery materials or Li-containing alloys, pose another set of challenges, including Ga implantation, Ga-induced alloying and segregation at grain boundaries, sample amorphization, and defect creation, along with the reactivity of Ga that can cause critical modifications of the sampled material (Belkacemi, et al., 2023; Gault, et al., 2023; Mayer, et al., 2007). Ga-induced beam damage at room temperature can be significant, although optimized preparation strategies can reduce it (Bassim, et al., 2012; Norris, 2019; Nowakowski, et al., 2017). More specifically, Ga ion implantation damage with cryogenic sample preparation of frozen liquids and biological samples is greatly reduced, as quantified in Lucas & Grigorieff (2023). The use of cryo-transfer shuttles helps in overcoming these issues and protects air-sensitive samples, which facilitates the APT analysis (Chang, et al., 2019; Chen, et al., 2021; Kim, Dong et al., 2022; Perea, et al., 2017).

Along with the specimen preparation, APT analysis of frozen liquids faces issues often reported arising from localized heating at the field evaporating surface (McCarroll et al., 2020; Kelly et al., 2009). Recent reports suggest that the use of thin conductive coatings led to an increase in yield by using, e.g., metals films or graphene (Larson et al., 2013; Seol et al., 2016; Adineh et al., 2018), suggesting that a free flow of charge at the surface of the specimen facilitates controlled field evaporation along with the heat extraction. Recent work also showed that a conductive coating on oxide materials significantly improved APT data quality and even enabled successful analysis of challenging materials (Kim, Antonov, et al., 2022; Kim et al., 2023; Seol et al., 2016). These approaches require exposition of the specimen to ambient conditions to insert them into a separate device for the deposition of the coating. As a response to the user community's needs, some commercial FIB systems now offer an *in situ* chamber sputter coater, and some third-party cryogenic sample transfer systems now include potentially standalone cryogenic sputter coating options (Klumpe, et al., 2022; Long, et al., 2022). An *in situ* coating was introduced by Kolling & Vandervorst (2009) by using redeposition inside the FIB, which was revisited by Douglas et al. (Douglas, et al., 2022) who used it to reinforce welds between sample and Si support by sputtering the W micromanipulator at cryogenic temperature.

Here, building on these methods, we introduce a workflow for APT specimen preparation under cryogenic conditions, from a glovebox to an FIB for site-specific lift-out, specimen sharpening, and *in situ* coating to an atom probe for analysis with cryogenic, ultrahigh vacuum (UHV) transfer. The workflow is demonstrated in the analysis of a ceramic, namely an anodized alumina membrane, a Cu-based alloy (dezincified brass), supported and unsupported frozen aqueous solutions, and finally commercial battery cathode oxides (NMC811) following the optimization of an *in situ* capping protocol. Our approach can be used on a wide range of microscopes, at cryogenic and room temperature, and allows protecting specimens from the exposure to ambient environment, which makes it of general interest across the community.

Materials and Methods

Materials

For the present study, specimens were produced from a range of materials systems; the details of the preparation are provided below in their respective sections.

Anodized alumina oxide (AAO) membrane with 80 nm pore size and 50 µm thickness was sourced from InRedox, Longmont CO, USA, electrodeposited with nickel following the procedure described in Lim et al. (2020).

Yellow brass (Cu: 63% and Zn: 37%) sheets with 0.4 mm thickness (Metall Ehrnsberger GbR, Teublitz Germany) were cut into 3 mm×7 mm pieces, annealed at 600°C for 1 h, and furnace cooled under argon. Subsequently, the brass was dezincified by annealing at 800°C under vacuum for 1 h and furnace cooled under vacuum.

For liquids, a solution of 200 mL type 1 deionized (DI) water (Sigma-Aldrich, St. Louis, MO, USA) and 5 g L-arginine hydrochloride (HCl) (Alfa Aesar, Kandel, Germany) was prepared. Phosphate buffered saline (PBS) solution, 0.1 mM concentration, was purchased from Sigma-Aldrich directly.

NMC811 ($LiNi_8Co_1Mn_1O_2$) battery cathode material was sourced from Targray (Kirkland, Canada).

FIB With Cryo-Stage

A Thermo-Fisher Helios 5 CX Gallium FIB/SEM (Thermo-Fisher Scientific, Waltham MA, USA) equipped with an Aquilos cryo-stage with free rotation capability and a Thermo-Fisher EZ-Lift tungsten cryogenic manipulator was used for specimen preparation. The stage can be cooled to a set point of −190°C and the manipulator to −175°C by a circulation of N_2 gas flow of 190 mg/s through a heat exchanger system within a liquid nitrogen Dewar. To cool the stage and the micromanipulator to the target temperature, 1 h is required to reach thermal equilibrium and avoid any drift during the subsequent preparation. In the following, all SEM images are shown with a red border, whereas ion beam images are delineated in blue.

A SylaTech glovebox (SylaTech GmbH, Walzbachtal, Germany) was used to maintain a level of moisture normally <20 ppm oxygen and a dew point of −98°C, for handling air-sensitive specimens and for plunge freezing into LN2. A dual post cryogenic atom probe puck (Cameca Instruments, Madison, WI, USA), e.g., one with two sitting holes which each accommodate a specimen holder with Cu springs ("Cu clip", Cameca) in opposite directions, was used to hold two clips, one with the bulk material. A commercial 36-microtip array Si coupon (Cameca FT 36) was used a support and is mounted on a Cu clip in one of the slots. Images of the dual puck are provided in Supplementary Figure S1.

Atom Probe Tomography

The APT measurements were conducted using a local electrode atom probe (LEAP, Cameca Instruments Inc.), either straight flight path (LEAP 5000 XS) or reflectron (LEAP 5000 XR). Measurements were done at different conditions depending on the samples. The reconstruction of the three-dimensional

atom maps and data analysis was carried out using the commercial software AP Suite 6.1.

Cryo-Lift-Out Workflow

As a preliminary step of this workflow, a cuboidal bar having dimensions 20 × 2 × 12 µm was extracted from bulk Cr piece using a FIB protocol described in Thompson et al. (2007). Cr was selected because it is widely available, is often used as a coating material for SEM or APT specimens, and was shown in previous works to exhibit good adhesion to flat and curved surfaces (Kölling & Vandervorst, 2009). The Cr-lamella was attached with the micromanipulator using Pt via. The GIS system and all steps were performed at room temperature, shown in Fig 1a. This attached Cr-lamella was later used during the subsequent stages of specimen preparation.

This attachment could also be performed at cryogenic temperature using the protocol described by Schreiber et al. (2018) if necessary. Another preliminary step done to increase the contact area of Si posts and trenched lamella, the top part of the flat post of the 3-µm-wide flat top Si microtip arrays is sliced at 0° degree tilt, shown in Figure 1b. The resulting angle to the normal to the surface is 38°.

For the cryo-lift-out, the stage was cooled to −190°C, and the micromanipulator was cooled to −175°C. A schematic of the step-by-step cryo-lift-out procedure is presented in Figure 2. The first step of the process involved locating the ROI and milling the adjoining regions leaving an ROI as a slice of 3–5 µm in thickness, very similar to those used for the well-established "lift-out" technique for transmission electron microscope (TEM) cross-section specimen preparation (Giannuzzi & Stevie, 1999), shown in Figure 2a. The sample was brought to 0° degree tilt to mill undercuts leaving the slice only attached to one edge. The micromanipulator attached with the Cr-lamella was then inserted and maneuvered close (<0.2 µm) to the trenched bar from the ROI. At this point, cuts for redeposition (Schreiber et al., 2018) were used to attach the Cr-lamella to the ROI. Six to eight line cuts with 4 µm length and cut depths of 1 µm were made using ion beam current of 80 pA at 30 kV, shown as white dashed lines in Figure 2b. The bar was then extracted from the bulk sample, leaving the ROI bar attached with Cr-lamella, as shown in Figure 2b.

In the next step, the bar was aligned to the top of presliced Si posts. The bar was then secured to the post using vertical line cuts (4–5 lines) for redeposition, using ion beam current of 80 pA at 30 kV, shown as vertical white dashed lines in Figure 2c. Once the weld was secured, the ion beam was used to slice the remaining bar from the mounted slice. This process was repeated to prepare multiple slices from a single lifted-out bar (Fig. 2c). Similar redeposition cuts were made from all sides by rotating the stage by 90°, at 0° tilt. This step fortified the bond between the slice and the post.

Next, a rectangular cut was made at the interface, roughly removing half of the thickness of the mounted slice (Fig. 2c). The Cr-lamella attached to the micromanipulator was maneuvered close to this cavity. Cr was ablated from the Cr-lamella using a current of 80 pA at 30 kV using regular cross-section with a cut depth of 1 µm, shown in yellow color in Figure 2d. Cr deposited in the cavity, at the interface between the sample and the Si post, and provided a strong bond analogous to the Pt in the conventional FIB-based preparation for APT specimens.

Suitable needle-shaped specimens were then obtained by applying a sequence of annular milling patterns to the specimen post in the FIB, where the outer diameter of the mill pattern was slightly larger than the outer diameter of the sample and the inner diameter gets continuously smaller. The stage was tilted to 52°, annular milling was performed, and the final specimens shaped as sharp needles were obtained as shown in Figure 2e.

Supplementary Table 1 lists all the currents used for the lift-out, which varied with the nature of the sample. Due to the reduced damage from Ga during cryo-preparations, no low kV (kilovolt) cleaning was performed.

Results and Discussion

Nickel-Coated AAO Membranes

Preparing a nickel-coated AAO membrane at cryogenic temperatures for analysis in a LEAP 5000 XS was an interesting case study. AAO membranes are used for the preparation of nanostructured materials and, because of their hydrophilicity, are ideal templates to hold liquids and freeze them for subsequent APT analyses. Coating the AAO membrane with nickel can improve its hydrophilic nature, which can make it easier to load sample onto the membrane. Alumina is a ceramic, which hence presents its own challenges for FIB-based preparations, i.e., charging, low milling rates, and APT analysis. And to demonstrate the versatility of this technique for ceramics, samples were prepared at cryogenic temperatures.

Figure 3a presents the top and Figure 3b the cross-sectional view of the AAO templates showing deposited Ni to a depth of ∼3 µm. This sample was attached to a commercial Cu clip along with a Si coupon in a dual cryo-puck and was transferred to the FIB.

Samples were prepared as per our abovementioned protocol at cryogenic temperatures, and the transfer to the atom probe was performed under cryogenic temperatures using the suitcase. For this particular set of experiments, redeposition welding was performed with yellow brass, rather than Cr. The specimens were run in laser pulsing mode at a base temperature of 50 K, laser energy of 100 pJ, and pulse repetition rate of 125 kHz with a detection rate of 1 ion per 1,000 pulses on average.

An X–Z cross-section from the APT reconstruction of an analysis from the bulk AAO material, showing a homogeneous distribution of aluminum and oxygen, is displayed in Figure 3c. A filled pore in the AAO material is visualized using an iso-concentration surface of 5 at. % Ni, Cu, and Zn in Figure 3d. The Cu in the nickel-filled pore can be explained by the presence of a small crack in that region of the AAO template, and when the APT specimen was fabricated, some brass was redeposited and integrated into the pore itself.

Cryo-FIB Preparation of Dezincified Brass

Dezincified yellow brass (initially Cu: 63% and Zn: 37%) was used as an example of metallic materials. Dezincification creates a nanoporous structure, which can serve as an affordable template to hold liquids for APT studies in comparison to nanoporous gold. Figure 4a shows the top and cross-sectioned view of the brass after dezincification.

The Si posts and the dezincified brass piece were mounted on copper clips in the dual puck and transferred to the FIB at room temperature. The FIB cryogenic stage was cooled to cryogenic temperatures, and atom probe specimens were prepared. After preparation, the stage was brought back to room temperature. The transfer to the atom probe was performed in ambient atmosphere. The measurement was performed at

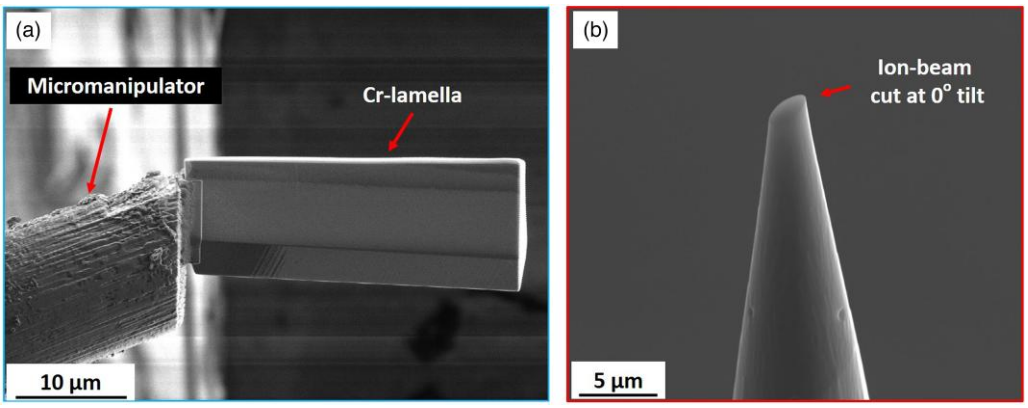

Fig. 1. (**a**) Ion beam image of the Cr-lamella lift-out. Pt welding was used, and the lift was done at room temperature. (**b**) Secondary electron beam image of the sliced Si micro post. Milling was performed at 0° degree tilt.

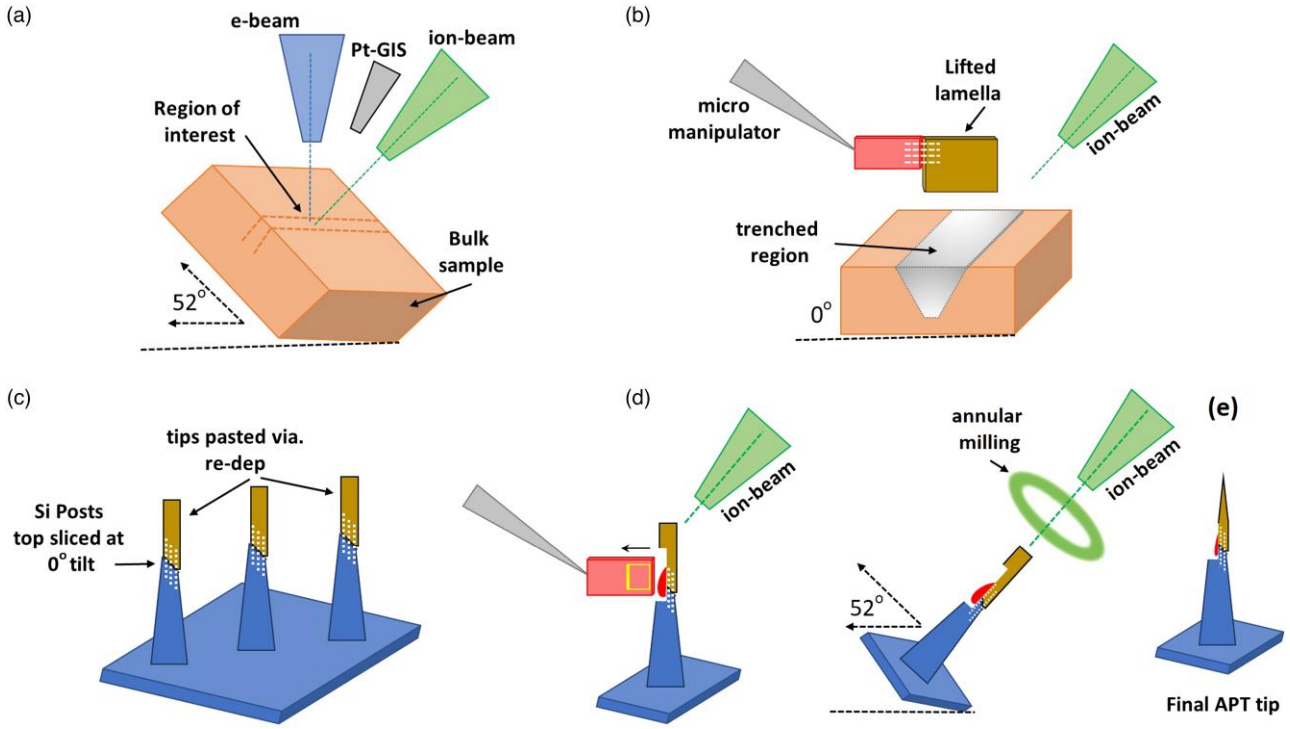

Fig. 2. Schematic showing step-by-step preparation of cryo-FIB sample preparations, developed in this work. (**a**) Initial lamella cuts (**b**) lifted-out lamella attached to Cr-lamella (**c**) lamella pieces attached to silicon micro-posts via redeposition welding (**d**) redeposition of Cr from Cr-lamella into gap etched into the silicon micropost (**e**) final annular milling and resultant tip.

50 K, with a laser pulse energy of 40 pJ at a pulse repetition rate of 200 kHz with a detection rate of 5 ions per 1,000 pulses on average. Figure 4b shows the (002) Cu pole in the detector event map. Slices through the APT reconstruction from the X–Y and X–Z planes are provided in Figures 4c and 4d, respectively. The bulk composition obtained from the whole tip suggests a Cu and Zn content of 87 and 13 at. %, respectively, indicative of the loss of Zn expected from the incomplete dezincification.

Frozen Liquids on Cu-Based Substrate

Previous reports of APT analysis of frozen aqueous solutions showed the importance of selecting a hydrophilic substrate to hold the liquid of interest (El-Zoka et al., 2020; Schwarz et al., 2020). The dezincified brass discussed above has nanoporosities which can hold aqueous solutions for freezing and APT specimen preparation. Here, a 0.1 M arginine hydrochloride solution was prepared and a droplet of 2 µL was placed on the surface using a pipette inside the glovebox and blotted as required. The dual puck, having Si micro posts on one clip and liquid on the second clip, was plunged in LN2 and subsequently transported from the glovebox into the FIB using the precooled Ferrovac suitcase, using the procedure in Stephenson et al. (2018).

Figures 5a to 5f detail the corresponding preparation process. The frozen liquid on dezincified brass was lifted-out, and the slice is mounted on the presliced Si posts as shown in Figure 5a. The lifted frozen liquid was mounted using redeposition cuts, and the attachment with the Si post was

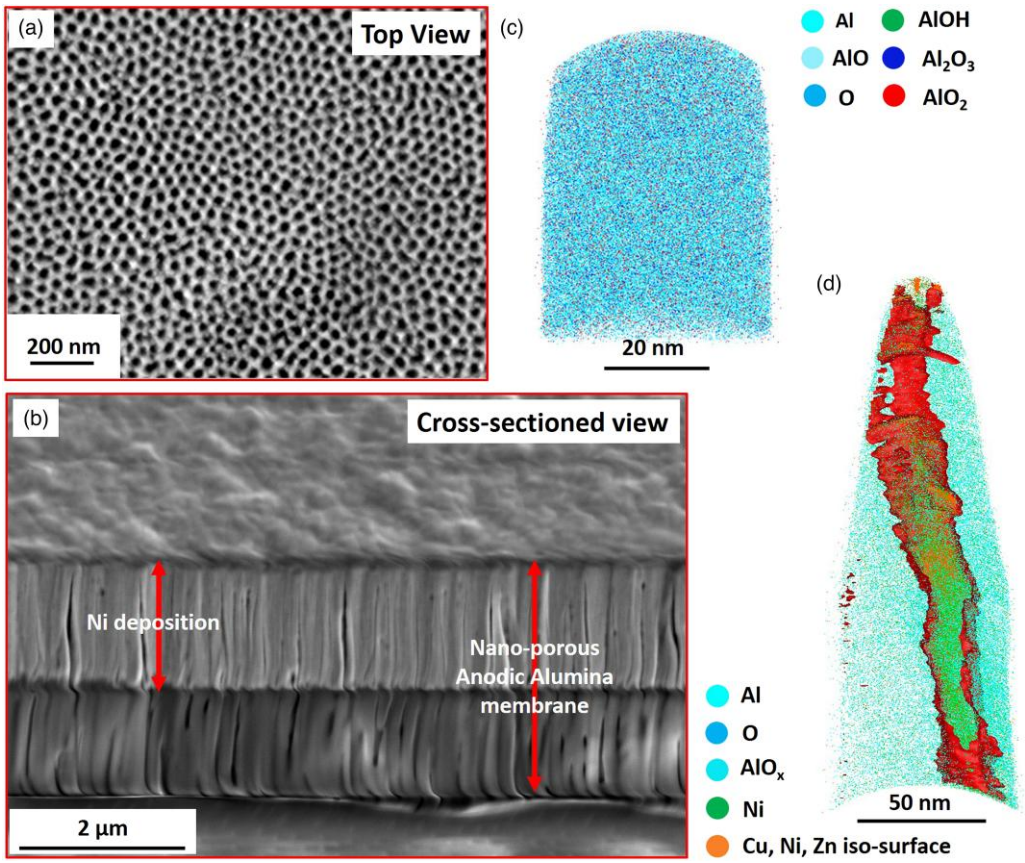

Fig. 3. (**a**) Top view and (**b**) cross-sectioned view of typical Ni-filled pore (bottom image). (**c**) X–Z cross-section slice of APT reconstruction of pure AAO. (**d**) X–Z cross-section of metal-filled pore in AAO in APT reconstruction, visualized as 5% atomic percent metal iso-surface (Ni + Cu + Zn).

done using redeposition cuts using a current of 40 pA at 30 kV with cut depth of 1 µm. Redeposition cuts are visible in Figure 5a. Figures 5b to 5c are top and side views of the mounted sample on Si. Figure 5d shows the side cut at the interface and the Cr deposition in the cavity to strengthen the bond, while Figure 5e displays the milled sample with water on top and then brass supported by the Si post. Figure 5f is the final prepared APT specimen of the frozen solution at a higher magnification. There is good contrast between the liquid layer and the metallic support material.

Specimens were transferred to LEAP 5000 XS using the pre-cooled UHV suitcase. Specimens were analyzed at a base temperature of 50 K, a laser pulse energy of 40 pJ, a repetition rate of 125 kHz, and a detection rate of 7 ions per 1,000 pulses on average. The corresponding APT mass spectrum is shown in Figure 6, and in the inset, the X–Y cross-section slice through the reconstruction is presented.

The carrier substrate contains Cu and Zn, and these two species appear to be detected as atomic and molecular ions in the mass spectrum. This may be due to issues with insufficient rinsing leaving behind some residues or the dissolution of surface oxides and hydroxides when the surface is wetted by the solution of interest. These species can then interfere with the identification of ions formed by fragmentation of organic molecules. These metallic species are detected across the entire data sets and not only on the edges, as could be expected if they originated by redeposition during FIB milling. A different substrate should be used to avoid mass interferences with these particular molecules.

Direct Lift-Out of Bulk Frozen Liquid Without Support

Direct, site-specific lift-out of liquids for APT analysis has not been demonstrated. There are reports of cryo-TEM sample preparation of frozen liquids (Mahamid et al., 2016; Schaffer et al., 2019); however, those methods rely on Pt-GIS for sample coating and welding. In an attempt to lift-out only frozen liquid (i.e., without substrate), we have prepared a solution using type I DI water and a dilute PBS aqueous solution. A deposited droplet of the liquid on a nanoporous Cu support was plunged into LN2 and inserted into the FIB through the suitcase. A rectangular lamella containing only the ice was cut, as shown in Figure 7a, and then, the lamella was extracted and welded to a Si post using redeposit cuts and Cr welds as described in Cryo-Lift-Out Workflow. The redeposit cut parameters were the same as used previously for the water on Cu substrate. The close-up in Figures 7b to 7c demonstrates the absence of the substrate, with the darker areas, particularly near the Si microtip, showing lower electron contrast than the Si microtip, thereby demonstrating that the specimen is lighter and not the metallic substrate.

While annular milling is typically performed for APT specimen preparation, in this specific case, it must be generally avoided. Frozen aqueous solutions mill at a much higher

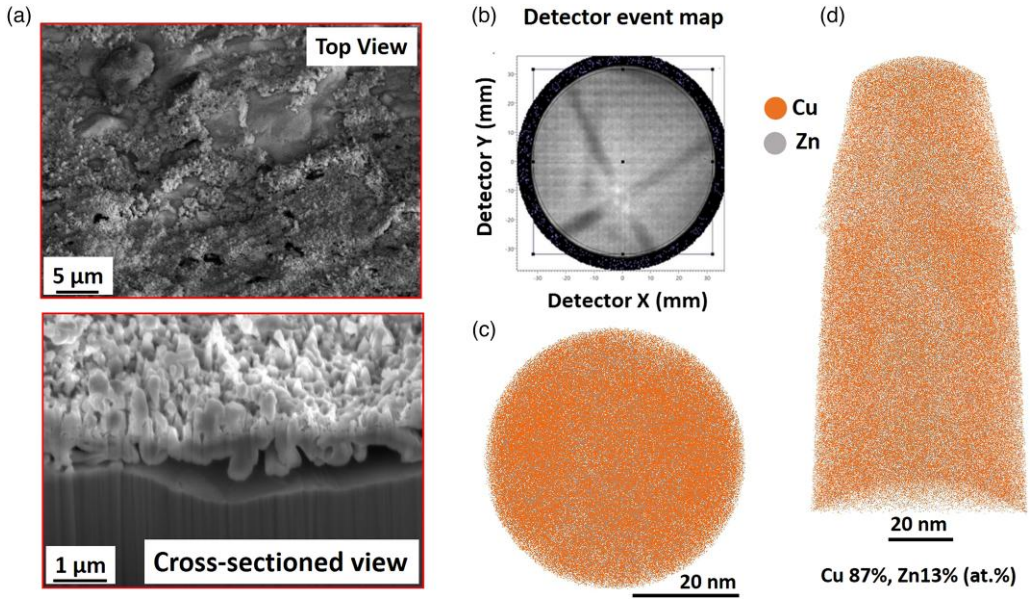

Fig. 4. (**a**) Top and cross-sectioned view of brass sample after dezincification. (**b**) Cu (002) pole in detector event map and APT reconstruction of low-zinc brass, after cryogenic sample preparation. (**c**) Y–Z slice. (**d**) X–Y slice.

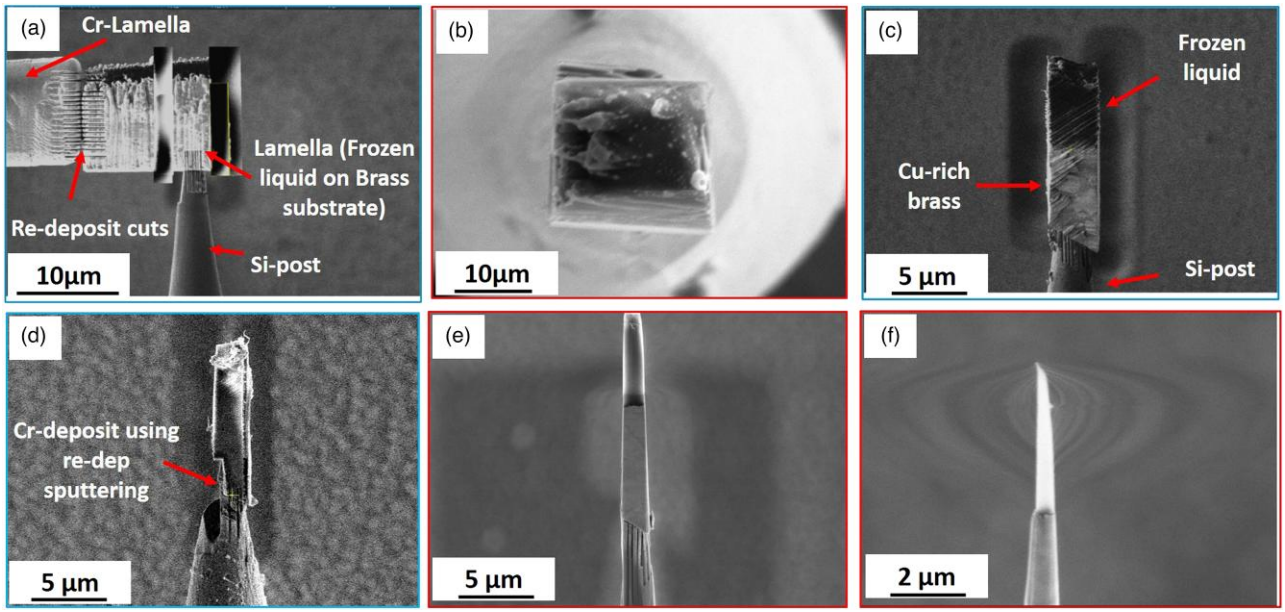

Fig. 5. Cryogenic APT specimen preparation procedure for a 0.1 M arginine HCl solution in type I ultrapure water on nonporous Cu. (**a**) FIB view, mounting ice on brass on Si microtip. (**b**) SEM view of mounted ice sample. (**c**) FIB cross-section view of ice APT specimen on brass. (**d**) Ion beam image showing the cavity milled at the interface of Si post and sample; Cr is deposited in the cavity. (**e**) Sharpened tip of ice and brass. (**f**) SEM view of final sharpened ice APT specimen.

rate than the underlying Si post, making it challenging not to mill through the entire layer and damage the redeposition weld, which would lower yield. Here, two rectangles were set at +5° and −5° tilt, as in Figure 7c, and directionally milled at 80 pA then 40 pA toward the interface rather than away from it for varying times (Larson et al., 1998). The stage was then rotated at 90°, and the procedure was repeated, making a tall pyramidal structure. Final annular milling was performed at 30 kV and 40 and 24 pA, and the image of the final specimen is shown in Figure 7d.

Specimens were analyzed in both voltage and laser modes. In Figure 8 a mass spectrum is plotted for a data set obtained containing ~1 million ions obtained at a base temperature of 50°K, a pulse fraction of 20%, a repetition rate of 200 kHz, and a detection rate of 1.5 ions per 1,000 pulses on average. It contains protonated water clusters $(H_2O)_nH^+$ where n is the number of the water molecules. An example of mass spectrum, obtained in laser pulsing mode, is shown in Figure 9. It contains 7 million ions, extracted from a larger data set, obtained at 50 K, a laser pulse energy of 66 pJ, a repetition rate of 100 kHz, and a detection rate of 5.5 ions per 1,000 pulses on average. This specific section was extracted from a larger data set, where acquisition parameters were being swept for optimization. The spectrum is dominated by similar water

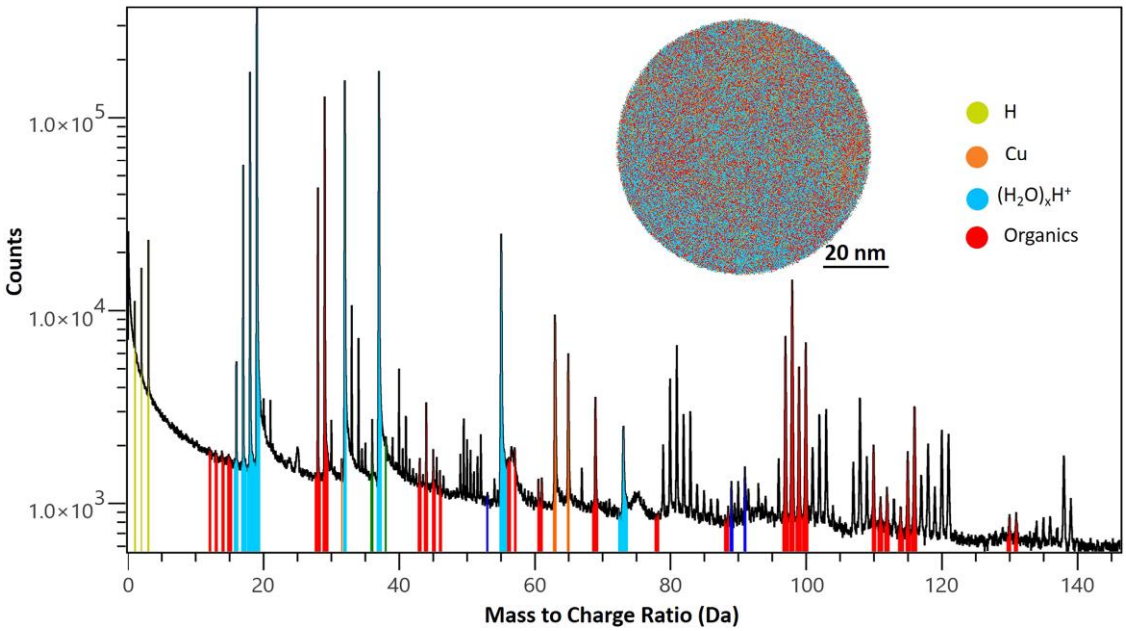

Fig. 6. Mass spectrum from the AA solution on support (inset) selected APT ion range X–Y view.

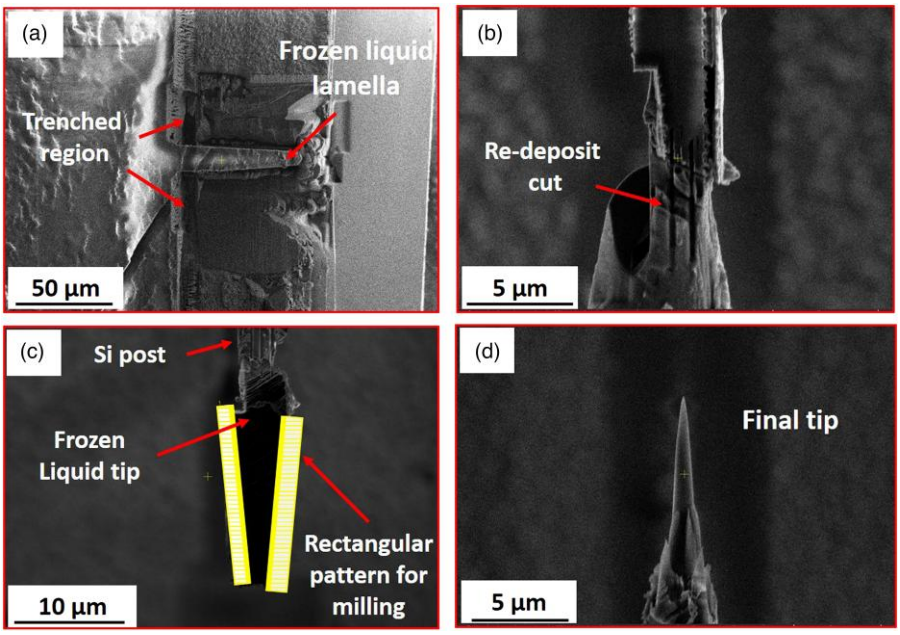

Fig. 7. Preparation procedure for pure water lamellas. (**a**) Bulk ice. (**b**) Pure water APT specimen, zoomed version of weld showing water down to Si interface. (**c**) Wedge sharpening of APT specimen; red arrows on the rectangles show milling direction. (**d**) Final sharpened APT specimen (rotated with respect to **c**).

clusters and a higher level of background. The higher thermal tails from the water clusters make it impossible to observe anything else in the mass spectra. In both cases, the molecular ions of water match previous work on metallic supports (El-Zoka et al., 2020; Schwarz et al., 2020) and from other groups looking at water in APT (Panitz, 1991) or desorption and ionization studies of water from sharp specimens, e.g., field emitters, under high field conditions (J.A.Panitz, 1992; Pinkerton, et al., 1999; Stuve, 2012). Larger laser mode data sets up to 40 million ions have been collected, demonstrating that the welding method works well. The spectrum reported in Figure 9 was from a significantly shorter APT specimen than the one shown in Figure 7d. It was ~4 µm tall (when measured from the highest edge of the Si micro post). In general, taller ice APT specimens have higher temperature rise and slower cooling, and the mass resolution and thermal tails for taller APT specimens are significantly worse. A significantly taller APT specimen, in excess of 10 µm, only showed water clusters to $n = 5$, indicative of a larger field drop as discussed by Stephenson et al. (2018).

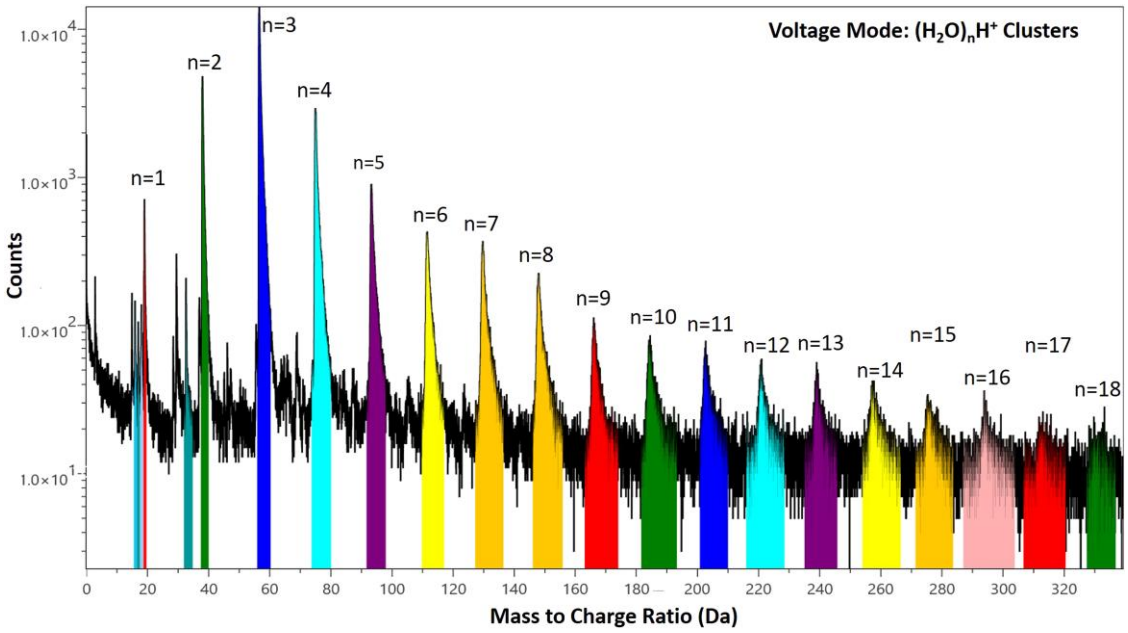

Fig. 8. Mass spectrum from the voltage mode run of frozen liquid APT specimen.

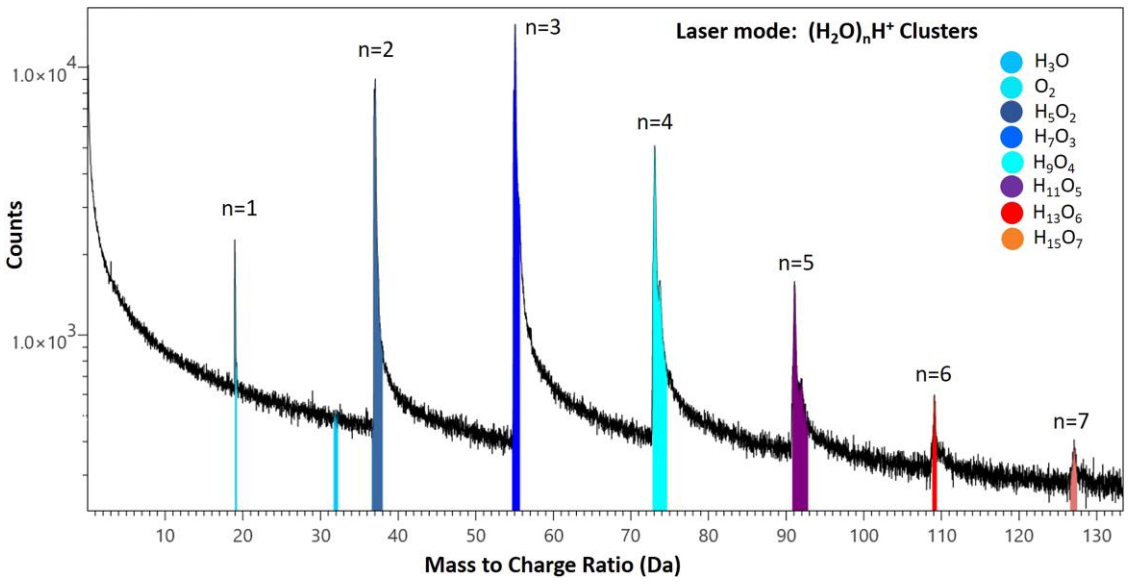

Fig. 9. Mass spectrum from the laser mode run of frozen liquid APT specimen.

NMC811 Battery Cathode Material

Battery materials tend to be air- and beam-sensitive, making specimen preparation and transport challenging. In addition, the diffusion of lithium ions (Li-ions) driven by the electrostatic field can result in homogeneous distribution of Li-ions (Pfeiffer et al., 2017; Greiwe et al., 2014). Kim et al. (Kim, Antonov, et al., 2022) proposed that the formation of a conductive thin layer would shield the electrostatic field conditions that facilitate early specimen fracture.

Specimens from a commercial battery cathode material, NMC811, were prepared at cryogenic temperature. In order to enable shielding, we aimed to deposit a thin metal film on the finally shaped specimens using the method introduced by Kölling & Vandervorst (2009). Different geometries of the Cr-lamella for redeposition sputtering on sharpened APT specimens, as shown in Figures 10a to 10c, were attempted. The results obtained from different geometries are shared in supplementary files. The most even coverage was obtained for the semicircular geometry, as shown in Figures 10c and 10d.

The micromanipulator with the attached Cr-lamella was brought to the center of the ion beam focus, and a semicircular (radius of 8 µm) cut was made using ion beam current of 0.23 nA at 30 kV, shown in Figure 10c. In the next step, the Cr-lamella with the semicircular cavity was maneuvered such that it aligned very close to the sharpened APT specimen. Subsequently, a semicircular pattern with an inner diameter of 8 µm and outer diameter of 11 µm was placed on the cavity,

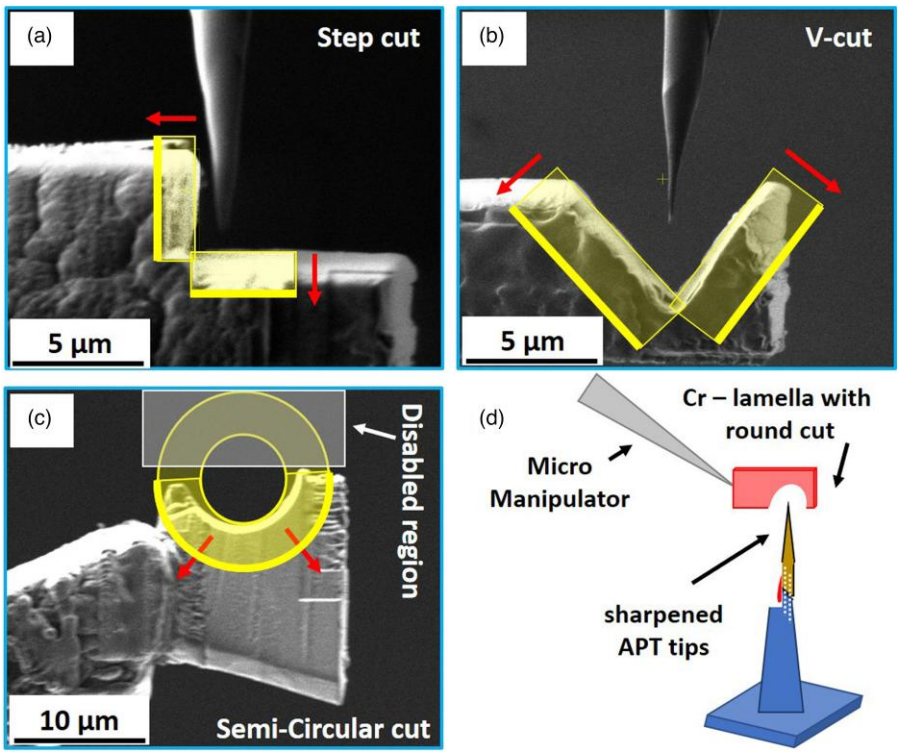

Fig. 10. Ion beam image for different geometries tried for redeposit geometries. (**a**) Step geometry, (**b**) V-cut geometry, and (**c**) semicircular cut geometry. (**d**) Schematic for the arrangement of the tip across the circular cut. The pattern used for redeposit sputtering is illustrated in yellow, and milling direction is marked with red arrows.

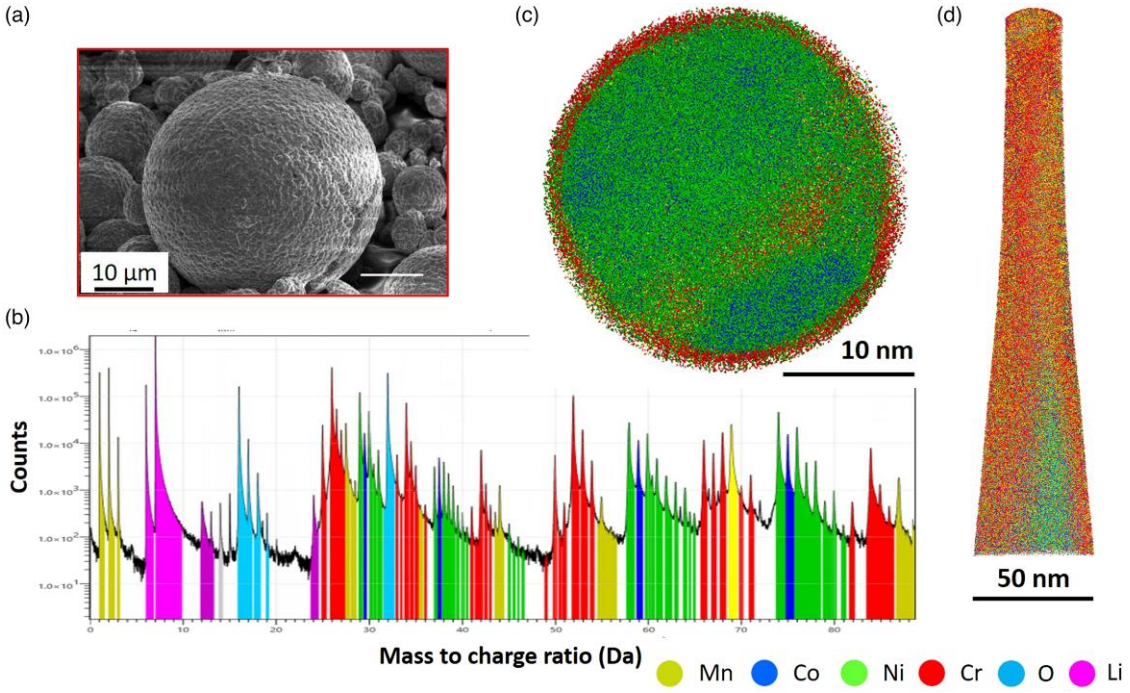

Fig. 11. (**a**) Secondary electron image of the NMC811 cathode powder sample, (**b**) mass spectrum obtained from APT run of the NMC tips, (**c**) APT reconstruction of the four-sided coated NMC tips and prepared using circular cuts on Cr-lamella (image is from the X–Y slice), and (**d**) visualization of the same tip from the Y–Z plane.

and to avoid the cutting of the prepared specimen, a rectangle with disabled milling was placed alongside the circular pattern. The milling was performed inside out with a current of 40 pA for 20 s. After that, the Cr-lamella was retracted and the stage was rotated by 90°, and the same procedure was repeated to cover the other sides of the APT specimen. To ensure proper coating, sputtering was performed from all four sides. The stage and coated APT tips were brought to room temperature.

Figure 11 shows a secondary electron micrograph of secondary particle from the NMC811 powder. *In situ* Cr-coated APT specimens were prepared from this particle, using the abovementioned methodology, and transferred into the atom probe through the suitcase. Figure 11b shows the mass spectrum from an APT analysis at a base temperature of 60°K, a laser pulse energy of 30 pJ, a pulse repetition rate of 125 kHz, and a detection rate of 8 ions per 1,000 pulses on average and shows clear peaks associated with Cr. APT reconstruction of the sample is presented in Figures 11c and 11d; a thin layer of Cr surrounds the imaged region. No signs of heterogeneous Li distribution associated with *in situ* delithiation are observed in this data set, despite the relatively high laser pulse energy used compared with reports by Kim et al. (2022).

Note that typically, the coating covers some but not all the specimen's length, particularly if these are several µm in length. Once the atom probe analysis moves into regions in which specimens are uncoated, field-induced lithium migration was seen to occur, similar to the data by Kim et al. (2022), which we believe is due to a lack of shielding and not only because the specimen is becoming blunter. More detailed work would also be necessary on this front. In principle, the specimen could be carried back into the FIB through the suitcase, and Cr deposited once again.

Conclusions and Future Work

Eyeing the future goals of enabling APT analyses for frozen wet samples, we demonstrate an efficient, reliable, and likely universal cryo-FIB-lift-out sample preparation technique for APT studies. Expanding the use of FIB-based specimen preparation at cryogenic temperatures will also enhance the quality of APT data. As an added advantage, the current workflow allows multiple APT specimens from a single lift-out from a selected ROI.

We showcased the application of this protocol to a wide range of samples, including metal, oxides, liquids, and beam-sensitive battery materials, for the preparation of specimens suitable for APT analysis.

Attaching specimens by redeposition cuts proves to be sturdy and efficient, potentially overcoming the issues with Pt-based GIS at cryogenic temperatures. Redeposition cuts can be performed both at room and cryo temperatures.

We demonstrated cryo-lift-out of frozen liquids with and without substrate using redeposition procedure. The prepared specimen was also analyzed by APT in both voltage and laser pulsing modes. The quality of the obtained mass spectra was encouraging, but further optimization is required in the future. We included the data for pure water and solutions only as a way to demonstrate that specimens can be prepared using this workflow, but more systematic work is necessary to really be in a position to provide meaningful comparisons across data sets and solutions, as was done, e.g., in Schwarz et al. (2021, 2022, 2020).

Specimen from the battery cathode materials was successfully prepared, coated with Cr from all sides at cryogenic temperatures. The corresponding APT results suggest that beam damage was avoided by cryo-preparation and delithiation was avoided using Cr coating.

In the future, we aim to perform site-specific grain boundary preparation, for instance. Optimization of coating material and thickness could be performed. With respect to direct lift-out of liquids, future work includes optimizing the length and shape of the APT specimens. Additionally, the use of different metals for the weld and *in situ* sputter coating will be explored to improve heat and electrical conductivity which currently remains a significant challenge.

Supplementary Material

To view supplementary material for this article, please visit https://doi.org/10.1093/micmic/ozad120.

Acknowledgments

We thank Uwe Tezins, Christian Broß, and Andreas Sturm for their support at the FIB and APT facilities at Max-Planck-Institut für Eisenforschung GmbH. We would like to thank Katja Angehangt, Monika Nellessen, and Christian Broß for their assistance with sample preparation.

Financial Support

E.V.W., S.-H.K., A.E.-Z., and B.G. are grateful for funding from the European Research Council (ERC) for the project SHINE (ERC-CoG) #771602. F.G. and B.G. are grateful for funding from the U.K. Engineering and Physical Sciences Research Council (EPSRC) under the grant #EP/V007661/1. T.M.S. and B.G. are grateful to the Deutsche Forschungsgemeinschaft (DFG) for funding through the Leibniz Award.

Conflict of Interest

The authors declare that they have no competing interest.

References

Adineh VR, Zheng C, Zhang Q, Marceau RKW, Liu B, Chen Y, Si KJ, Weyland M, Velkov T, Cheng W, Li J & Fu J (2018). Graphene-enhanced 3D chemical mapping of biological specimens at near-atomic resolution. *Adv Funct Mater* **28**, 1801439. https://doi.org/10.1002/adfm.201801439

Bassim ND, De Gregorio BT, Kilcoyne ALD, Scott K, Chou T, Wirick S, Cody G & Stroud RM (2012). Minimizing damage during FIB sample preparation of soft materials. *J Microsc* **245**, 288–301. https://doi.org/10.1111/j.1365-2818.2011.03570.x

Belkacemi LT, Gault B, Esin VA & Epp J (2023). Ga-induced delithiation of grain boundaries in a Li containing Al-based alloy. *Mater Charact* **199**:112812. https://doi.org/10.1016/j.matchar.2023.112812

Cavalier A, Spehner D & Humbel BM (2008). *Handbook of Cryo-Preparation Methods for Electron Microscopy*. Boca Raton, FL: CRC Press.

Chang Y, Lu W, Guénolé J, Stephenson LT, Szczpaniak A, Kontis P, Ackerman AK, Dear FF, Mouton I, Zhong X, Zhang S, Dye D, Liebscher CH, Ponge D, Korte-Kerzel S, Raabe D & Gault B (2019). Ti and its alloys as examples of cryogenic focused ion beam milling of environmentally-sensitive materials. *Nat Commun* **10**, 942. https://doi.org/10.1038/s41467-019-08752-7

Chen Y-S, Griffith MJ & Cairney JM (2021). Cryo atom probe: Freezing atoms in place for 3D mapping. *Nano Today* **37**, 101107. https://doi.org/10.1016/j.nantod.2021.101107

Chen Y-S, Haley D, Gerstl SSA, London AJ, Sweeney F, Wepf RA, Rainforth WM, Bagot PAJ & Moody MP (2017). Direct observation of individual hydrogen atoms at trapping sites in a ferritic steel. *Science* **355**, 1196–1199. https://doi.org/10.1126/science.aal2418

De Geuser F & Gault B (2020). Metrology of small particles and solute clusters by atom probe tomography. *Acta Mater* **188**, 406–415. https://doi.org/10.1016/j.actamat.2020.02.023

Devaraj A, Perea DE, Liu J, Gordon LM, Prosa TJ, Parikh P, Diercks DR, Meher S, Kolli RP, Meng YS & Thevuthasan S (2018). Three-dimensional nanoscale characterisation of materials by atom probe tomography. *Int Mater Rev* **63**, 68–101. https://doi.org/10.1080/09506608.2016.1270728

Douglas JO, Conroy M, Giuliani F & Gault B (2022). In-situ sputtering from the micromanipulator to enable cryogenic preparation of specimens for atom probe tomography by focused-ion beam. http://arxiv.org/abs/2211.06877 (Accessed March 14, 2023).

Dubochet J & McDowall AW (1981). Vitrification of pure water for electron microscopy. *J Microsc* **124**(3), 3–4. https://doi.org/10.1111/j.1365-2818.1981.tb02483.x

El-Zoka AA, Kim S-H, Deville S, Newman RC, Stephenson LT & Gault B (2020). Enabling near-atomic–scale analysis of frozen water. *Sci Adv* **6**, eabd6324. https://doi.org/10.1126/sciadv.abd6324

Gault B, Chiaramonti A, Cojocaru-Mirédin O, Stender P, Dubosq R, Freysoldt C, Makineni SK, Li T, Moody M & Cairney JM (2021). Atom probe tomography. *Nat Rev Methods Primers* **1**, 1–30. https://doi.org/10.1038/s43586-021-00047-w

Gault B, Khanchandani H, Prithiv TS, Antonov S & Britton TB (2023). Transmission Kikuchi diffraction mapping induces structural damage in atom probe specimens. *Microsc Microanal* **29**(3), 1026–1036. https://doi.org/10.1093/micmic/ozad029

Gault B, Vurpillot F, Vella A, Gilbert M, Menand A, Blavette D & Deconihout B (2006). Design of a femtosecond laser assisted tomographic atom probe. *Rev Sci Instrum* **77**, 043705. https://doi.org/10.1063/1.2194089

Gerstl SSA & Wepf R (2015). Methods in creating, transferring, & measuring cryogenic samples for APT. *Microsc Microanal* **21**, 517–518. https://doi.org/10.1017/S1431927615003384

Giannuzzi LA & Stevie FA (1999). A review of focused ion beam milling techniques for TEM specimen preparation. *Micron* **30**, 197–204. https://doi.org/10.1016/S0968-4328(99)00005-0

Greiwe G-H, Balogh Z & Schmitz G (2014). Atom probe tomography of lithium-doped network glasses. *Ultramicroscopy* **141**, 51–55. https://doi.org/10.1016/j.ultramic.2014.03.007

Hono K, Ohkubo T, Chen YM, Kodzuka M, Oh-ishi K, Sepehri-Amin H, Li F, Kinno T, Tomiya S & Kanitani Y (2011). Broadening the applications of the atom probe technique by ultraviolet femtosecond laser. *Ultramicroscopy* **111**, 576–583. https://doi.org/10.1016/j.ultramic.2010.11.020

Kelly TF, Nishikawa O, Panitz JA & Prosa TJ (2009). Prospects for nanobiology with atom-probe tomography. *MRS Bulletin* **34**, 744–749. https://doi.org/10.1557/mrs2009.249

Kim SH, Antonov S, Zhou X, Stephenson LT, Jung C, El-Zoka AA, Schreiber DK, Conroy M & Gault B (2022). Atom probe analysis of electrode materials for Li-ion batteries: Challenges and ways forward. *J Mater Chem A* **10**, 4926–4935. https://doi.org/10.1039/D1TA10050E

Kim S-H, Dong K, Zhao H, El-Zoka AA, Zhou X, Woods EV, Giuliani F, Manke I, Raabe D & Gault B (2022). Understanding the degradation of a model Si anode in a Li-ion battery at the atomic scale. *J Phys Chem Lett* **13**, 8416–8421. https://doi.org/10.1021/acs.jpclett.2c02236

Kim S-H, El-Zoka AA & Gault B (2022). A liquid metal encapsulation for analyzing porous nanomaterials by atom probe tomography. *Microsc Microanal* **28**, 1198–1206. https://doi.org/10.1017/S1431927621012964

Kim S-H, Shin K, Zhou X, Jung C, Kim HY, Pedrazzini S, Conroy M, Henkelman G & Gault B (2023). Atom probe analysis of BaTiO3 enabled by metallic shielding. *Scr Mater* **229**, 115370. https://doi.org/10.1016/j.scriptamat.2023.115370

Kim S-H, Stephenson LT, da Silva AK, Gault B & El-Zoka AA (2022). Phase separation and anomalous shape transformation in frozen microscale eutectic indium-gallium upon remelting. *Materialia* **26**, 101595. https://doi.org/10.1016/j.mtla.2022.101595

Klumpe S, Kuba J, Schioetz OH, Erdmann PS, Rigort A & Plitzko JM (2022). Recent advances in gas injection system-free cryo-FIB lift-out transfer for cryo-electron tomography of multicellular organisms and tissues. *Micros Today* **30**(1), 42–47. https://doi.org/10.1017/S1551929521001528

Kölling S & Vandervorst W (2009). Failure mechanisms of silicon-based atom-probe tips. *Ultramicroscopy* **109**, 486–491. https://doi.org/10.1016/j.ultramic.2008.11.013

Larson DJ, Foord DT, Petford-Long AK, Anthony TC, Rozdilsky IM, Cerezo A & Smith GWD (1998). Focused ion-beam milling for field-ion specimen preparation: Preliminary investigations. *Ultramicroscopy* **75**, 147–159. https://doi.org/10.1016/S0304-3991(98)00058-8

Larson DJ, Prosa TJ, Bunton JH, Olson DP, Lawrence DF, Oltman E, Strennin SN & Kelly TF (2013). Improved mass resolving power and yield in atom probe tomography. *Microsc Microanal* **19**, 994–995. https://doi.org/10.1017/S143192761300696X

Li T, Devaraj A & Kruse N (2022). Atomic-scale characterization of (electro-)catalysts and battery materials by atom probe tomography. *Cell Rep Phys Sci* **3**, 101188. https://doi.org/10.1016/j.xcrp.2022.101188

Lim J, Kim S-H, Aymerich Armengol R, Kasian O, Choi P-P, Stephenson LT, Gault B & Scheu C (2020). Atomic-scale mapping of impurities in partially reduced hollow TiO_2 nanowires. *Angew Chem Int Ed* **59**, 5651–5655. https://doi.org/10.1002/anie.201915709

Long DM, Singh MK, Small KA & Watt J (2022). Cryo-FIB for TEM investigation of soft matter and beam sensitive energy materials. *Nanotechnology* **33**(50), 503001. https://doi.org/10.1088/1361-6528/ac92eb

Lucas BA & Grigorieff N (2023). Quantification of gallium cryo-FIB milling damage in biological lamellae. *Proc Natl Acad Sci U S A* **120**(23), e2301852120. https://doi.org/10.1073/pnas.2301852120

Mahamid J, Pfeffer S, Schaffer M, Villa E, Danev R, Kuhn Cuellar L, Förster F, Hyman AA, Plitzko JM & Baumeister W (2016). Visualizing the molecular sociology at the HeLa cell nuclear periphery. *Science* **351**, 969–972. https://doi.org/10.1126/science.aad8857

Marko M, Hsieh C, Moberlychan W, Mannella CA & Frank J (2006). Focused ion beam milling of vitreous water: Prospects for an alternative to cryo-ultramicrotomy of frozen-hydrated biological samples. *J Microsc* **222**(Pt 1), 42–47. https://doi.org/10.1111/j.1365-2818.2006.01567.x

Mayer J, Giannuzzi LA, Kamino T & Michael J (2007). TEM sample preparation and FIB-induced damage. *MRS Bulletin* **32**(5), 400–407. https://doi.org/10.1557/mrs2007.63

McCarroll IE, Bagot PAJ, Devaraj A, Perea DE & Cairney JM (2020). New frontiers in atom probe tomography: A review of research enabled by cryo and/or vacuum transfer systems. *Mater Today Adv* **7**, 100090. https://doi.org/10.1016/j.mtadv.2020.100090

Norris SR (2019). A comparison of beam-induced damage from xenon and gallium focused ion beams. In *Materials Science and Engineering*, pp. 43. Hamilton, Ontario: Canada McMaster University.

Nowakowski P, Bonifacio CS, Campin MJ, Ray ML & Fischione PE (2017). Accurate removal of implanted gallium and amorphous damage from TEM specimens after focused ion beam (FIB) preparation. *Microsc Microanal* **23**(S1), 300–301. https://doi.org/10.1017/S1431927617002185

Parmenter C, Fay M, Hartfield C, Amador G & Moldovan G (2014). Cryogenic FIB lift-out as a preparation method for damage-free soft matter TEM imaging. *Microsc Microanal* **20**, 1224–1225. https://doi.org/10.1017/S1431927614007855

Perea DE, Gerstl SSA, Chin J, Hirschi B & Evans JE (2017). An environmental transfer hub for multimodal atom probe tomography. *Adv Struct Chem Imaging* **3**, 12. https://doi.org/10.1186/s40679-017-0045-2

Perea DE, Schreiber DK, Wirth M & Evans JE (2019). Advanced FIB-based preparation of cryogenically-prepared specimens for APT analysis. *Microsc Microanal* **25**(S2), 878–879. https://doi.org/10.1017/S1431927619005129

Pfeiffer B, Maier J, Arlt J & Nowak C (2017). In situ atom probe deintercalation of lithium-manganese-oxide. *Microsc Microanal* **23**, 314–320. https://doi.org/10.1017/S1431927616012691

Pinkerton TD, Scovell DL, Johnson AL, Xia B, Medvedev V & Stuve EM (1999). Electric field effects in ionization of water–ice layers

on platinum. *Langmuir* **15**, 851–856. https://doi.org/10.1021/la980924o

Prosa TJ & Larson DJ (2017). Modern focused-ion-beam-based site-specific specimen preparation for atom probe tomography. *Microsc Microanal* **23**, 194–209. https://doi.org/10.1017/S1431927616012642

Qiu S, Garg V, Zhang S, Chen Y, Li J, Taylor A, Marceau RKW & Fu J (2020). Graphene encapsulation enabled high-throughput atom probe tomography of liquid specimens. *Ultramicroscopy* **216**, 113036. https://doi.org/10.1016/j.ultramic.2020.113036

Rivas NA, Babayigit A, Conings B, Schwarz T, Sturm A, Manjón AG, Cojocaru-Mirédin O, Gault B & Renner FU (2020). Cryo-focused ion beam preparation of perovskite based solar cells for atom probe tomography. *PLoS One* **15**, e0227920. https://doi.org/10.1371/journal.pone.0227920

Schaffer M, Pfeffer S, Mahamid J, Kleindiek S, Laugks T, Albert S, Engel BD, Rummel A, Smith AJ, Baumeister W & Plitzko JM (2019). A cryo-FIB lift-out technique enables molecular-resolution cryo-ET within native *Caenorhabditis elegans* tissue. *Nat Methods* **16**, 757–762. https://doi.org/10.1038/s41592-019-0497-5

Schreiber DK, Perea DE, Ryan JV, Evans JE & Vienna JD (2018). A method for site-specific and cryogenic specimen fabrication of liquid/solid interfaces for atom probe tomography. *Ultramicroscopy* **194**, 89–99. https://doi.org/10.1016/j.ultramic.2018.07.010

Schwarz TM, Dietrich CA, Ott J, Weikum EM, Lawitzki R, Solodenko H, Hadjixenophontos E, Gault B, Kästner J, Schmitz G & Stender P (2021). 3D sub-nanometer analysis of glucose in an aqueous solution by cryo-atom probe tomography. *Sci Rep* **11**(1), 11607. https://doi.org/10.1038/s41598-021-90862-8

Schwarz TM, Ott J, Solodenko H, Schmitz G & Stender P (2022). Nanoscale analysis of frozen honey by atom probe tomography. *Sci Rep* **12**(1), 17786. https://doi.org/10.1038/s41598-022-22717-9

Schwarz TM, Weikum EM, Meng K, Hadjixenophontos E, Dietrich CA, Kästner J, Stender P & Schmitz G (2020). Field evaporation and atom probe tomography of pure water tips. *Sci Rep* **10**, 20271. https://doi.org/10.1038/s41598-020-77130-x

Seol J-B, Kwak C-M, Kim Y-T & Park C-G (2016). Understanding of the field evaporation of surface modified oxide materials through transmission electron microscopy and atom probe tomography. *Appl Surf Sci* **368**, 368–377. https://doi.org/10.1016/j.apsusc.2016.01.196

Singh MP, Kim S-H, Zhou X, Kwak H, Kwiatkowski da Silva A, Antonov S, Aota LS, Jung C, Jung YS & Gault B (2023). Near-atomic-scale evolution of the surface chemistry in Li[Ni, Mn, Co]O2 cathode for Li-ion batteries stored in air. *Adv Energy Sustainability Res* **4**, 2200121. https://doi.org/10.1002/aesr.202200121

Stender P, Solodenko H, Weigel A, Balla I, Schwarz TM, Ott J, Roussell M, Joshi Y, Duran R, Al-Shakran M, Jacob T & Schmitz G (2022). A modular atom probe concept: Design, operational aspects, and performance of an integrated APT-FIB/SEM solution. *Microsc Microanal* **28**, 1168–1180. https://doi.org/10.1017/S1431927621013982

Stephenson LT, Szczepaniak A, Mouton I, Rusitzka KAK, Breen AJ, Tezins U, Sturm A, Vogel D, Chang Y, Kontis P, Rosenthal A, Shepard JD, Maier U, Kelly TF, Raabe D & Gault B (2018). The Laplace project: An integrated suite for preparing and transferring atom probe samples under cryogenic and UHV conditions. *PLoS One* **13**, e0209211. https://doi.org/10.1371/journal.pone.0209211

Stintz A & Panitz JA (1991). Imaging atom-probe analysis of an aqueous interface. *J Vac Sci Technol* **9**, 1365–1367. https://doi.org/10.1116/1.577628

Stintz A & Panitz JA (1992). Isothermal ramped field-desorption of water from metal surfaces. *J Appl Phys* **74**, 741–745. https://doi.org/10.1063/1.351860

Stuve EM (2012). Ionization of water in interfacial electric fields: An electrochemical view. *Chem Phys Lett* **519–520**, 1–17. https://doi.org/10.1016/j.cplett.2011.09.040

Thompson K, Lawrence D, Larson DJ, Olson JD, Kelly TF & Gorman B (2007). In situ site-specific specimen preparation for atom probe tomography. *Ultramicroscopy* **107**, 131–139. https://doi.org/10.1016/j.ultramic.2006.06.008

Zhang S, Gervinskas G, Qiu S, Venugopal H, Marceau RKW, de Marco A, Li J & Fu J (2022). Methods of preparing nanoscale vitreous ice needles for high-resolution cryogenic characterization. *Nano Lett* **22**, 6501–6508. https://doi.org/10.1021/acs.nanolett.2c01495

Zhao H, Chakraborty P, Ponge D, Hickel T, Sun B, Wu C-H, Gault B & Raabe D (2022). Hydrogen trapping and embrittlement in high-strength Al alloys. *Nature* **602**, 437–441. https://doi.org/10.1038/s41586-021-04343-z

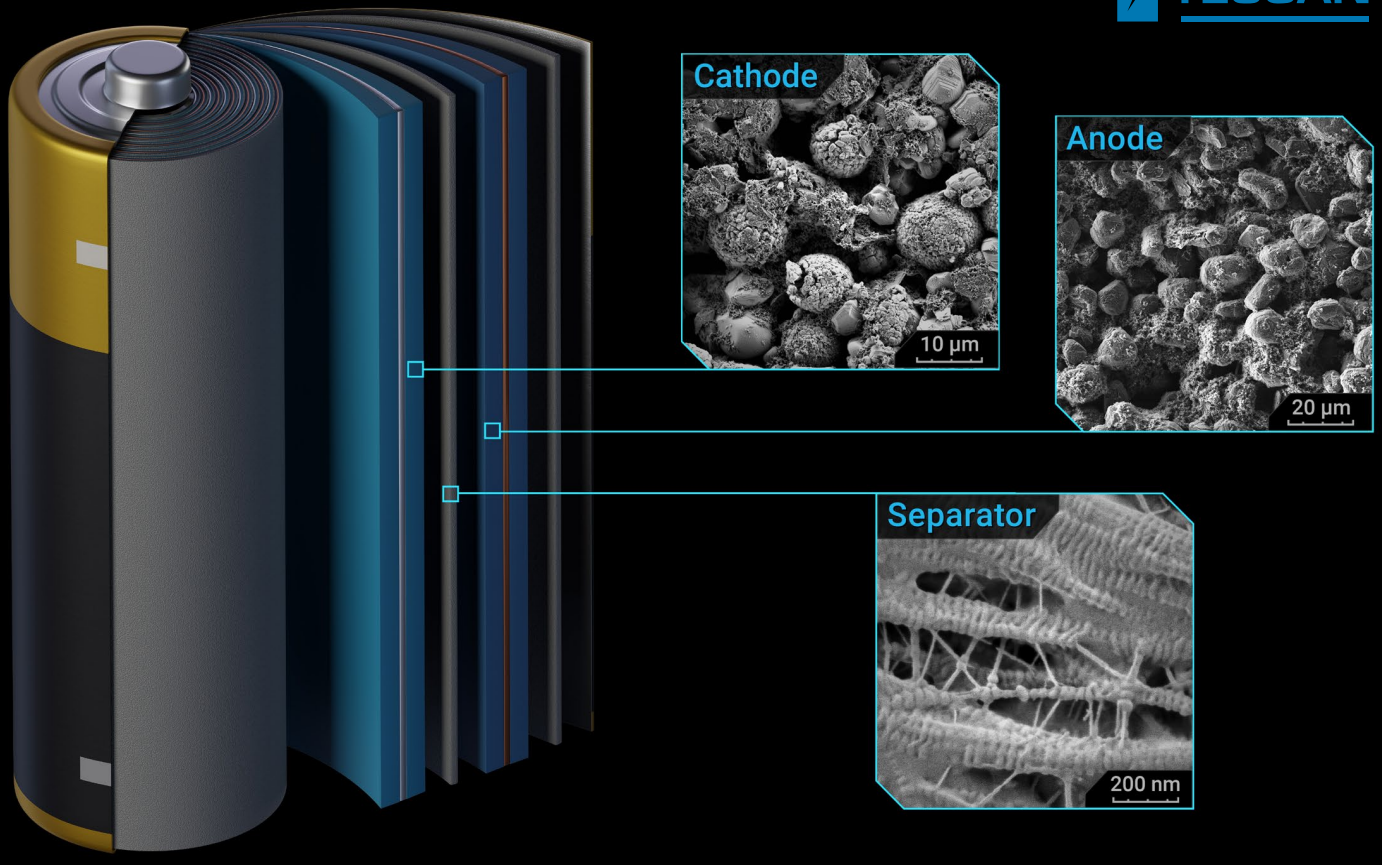

TESCAN Solutions for Battery Industry

Power your Advanced Battery Technology and Research with TESCAN Solutions

info.tescan.com/batteries

Scan for more information